Osteoimmunomodulatory potential of 3D printed submicron patterns assessed in a direct co-culture model

Nouri-Goushki, M.; Eijkel, B. I.M.; Minneboo, M.; Fratila-Apachitei, L. E.; Zadpoor, A. A.

DOI
10.1016/j.bioadv.2022.212993

Publication date
2022

Document Version
Final published version

Published in
Biomaterials Advances

139 (2022) 212993

Contents lists available at ScienceDirect

Biomaterials Advances

journal homepage: www.journals.elsevier.com/materials-science-and-engineering-c

Osteoimmunomodulatory potential of 3D printed submicron patterns assessed in a direct co-culture model

M. Nouri-Goushki [*,1], B.I.M. Eijkel [1], M. Minneboo, L.E. Fratila-Apachitei [*], A.A. Zadpoor

Department of Biomechanical Engineering, Faculty of Mechanical, Maritime, and Materials Engineering, Delft University of Technology (TU Delft), Mekelweg 2, 2628 CD Delft, the Netherlands

ARTICLE INFO

Keywords:
Osteoimmunomodulation
Submicron pillars
Immunoengineering
Additive manufacturing

ABSTRACT

Modulation of the immune response following the implantation of biomaterials can have beneficial effects on bone regeneration. This involves complex interactions between the inflammatory and osteogenic cells. Therefore, the study of cell-cell interactions using direct co-culture models integrated with biomaterials is of great interest. This research aimed to study the viability, morphology, and osteogenic activity of preosteoblasts (OBs) co-cultured with pro-inflammatory macrophages (M1s) on the 3D printed (non)patterned surfaces. OBs and M1s remained alive and proliferated actively for 14 days in the mixture of Dulbecco's Modified Eagle's Medium (DMEM) and alpha Minimum Essential Medium (α-MEM) (1:1), regardless of the cell ratio in the co-cultures. The spatial organization of the two types of cells changed with the time of culture from an initially uniform cell distribution to the formation of a thick layer of OBs covered by clusters of M1s. On day 7, the expression of PGE2 and TNF-α were upregulated in the co-culture relative to the mono-culture of OBs and M1s. The inflammation decreased differentiation and matrix mineralization of OBs after 28 days of culture. Interestingly, the incorporation of 3D printed submicron pillars into the direct co-culture model enhanced the differentiation of preosteoblasts, as shown by relatively higher RUNX2 expression, thereby revealing the osteoimmunomodulatory potential of such surface patterns.

1. Introduction

Upon implantation, biomaterials invariably elicit an inflammatory response. The type, severity, and evolution of this inflammatory response are dependent on the properties of the implanted biomaterial. Recently, there has been increasing evidence suggesting that biomaterials can actively modulate the response of inflammatory cells with potentially favorable effects on osteogenesis [1]. Such an osteoimmunomodulatory (OIM) process involves complex surface-cell and cell-cell interactions that require suitable *in vitro* cell culture models to be studied [2].

Among the various kinds of cells involved in OIM, macrophages play a major role. Since macrophages can be polarized towards both pro-inflammatory (M1) and prohealing (M2) phenotypes, a timely M1-to-M2 switch is required to prevent acute inflammation and promote tissue healing [1]. The specific molecules secreted by M1/M2 macrophages, such as transforming growth factor β (TGF-β), prostaglandin E2 (PGE2), and tumor necrosis factor α (TNF-α) can influence the fate of bone cells [1]. TNF-α is reported to hinder the differentiation of preosteoblast cells (OBs) by binding to TNF-α receptors in OBs [3] and suppressing the expression of bone morphogenetic protein 2 (BMP2) [4,5]. Furthermore, a high concentration of TNF-α in conditioned medium (CM) is reported to enhance the production of PGE2 in preosteoblasts, thereby promoting bone resorption [6]. At physiological concentrations, however, the matrix mineralization by mesenchymal stromal cells (MSCs) has been shown to be upregulated in the presence of four inflammatory cytokines, namely TNF-α, interferon gamma (IFN-γ), interleukin-17 (IL-17), and TGF-β [7]. Under such physiological conditions, TNF-α activates the nuclear factor kappa-light-chain-enhancer of activated B cells (NF-κB), consequently promoting the expression of osteogenic proteins, such as BMP2 and alkaline phosphatase (ALP) [7–10]. The effects of inflammatory cytokines on bone regeneration are, therefore, both dose- and time-dependent [7]. Unraveling the landscape of such dependencies requires co-culture models that are geared towards the study of such OIM responses.

Indirect and direct co-culture models are currently being used to

* Corresponding authors.
E-mail addresses: m.nourigoushki@tudelft.nl (M. Nouri-Goushki), E.L.Fratila-Apachitei@tudelft.nl (L.E. Fratila-Apachitei).
[1] Joint first authors

https://doi.org/10.1016/j.bioadv.2022.212993
Received 11 February 2022; Received in revised form 24 May 2022; Accepted 13 June 2022
Available online 15 June 2022

study OIM [11]. In indirect co-culture models, either the target cells are exposed to the conditioned media of the other cell type [12] or a barrier, such as a membrane [13], hydrogel [14], or transwell systems [15], is used to physically separate the different cell types [12,16]. This type of models have been most widely used due to their simplicity and effectiveness in studying paracrine signaling pathways [12]. Indirect co-culture models, however, exclude any direct communications between different cell types. Furthermore, it is difficult to reproduce the concentration of secreted factors in the conditioned medium [11,16]. In direct co-culture models, different cell types can be seeded simultaneously or in sequence [11]. Direct co-culture models can, therefore, better mimic the *in vivo* conditions. Nevertheless, distinguishing the function of each cell type is more complicated in such models and the distributions of all cell types need to be controlled [11].

Direct co-culture studies of the interactions between macrophages and (pre)osteoblasts/MSCs in the presence of topographies are currently very limited [17,18]. In one such study, the adhesion of osteoblasts on the titania surface is found to be inhibited in direct co-culture with macrophages [17]. The same study found that titania surfaces coated with non-mulberry silk fibroins enhance the mineralization of osteoblasts and reduce the expression of the inflammatory cytokine TNF-α in macrophages [17]. Surface topographies can provide physical cues that have been found to affect the paracrine interactions of MSCs with macrophages [18]. For example, MSCs seeded on microporous topographies (2 μm < pores diameter < 25 μm) have been shown to promote the expression of anti-inflammatory cytokines (interleukin-10 (IL-10)) in macrophages and attenuate the activity of bone resorption mediators [18].

In our previous studies, we investigated the role of 3D printed submicron pillars [19] on the inflammatory response of macrophages [20] and the osteogenic response of preosteoblasts [21] in mono-cultures. We observed that arrays of submicron pillars with specific sizes and spatial arrangement could promote the polarization of M1 macrophages towards prohealing M2 phenotype and enhance the expression of osteopontin (OPN) in both osteogenic and non-osteogenic media [20,21]. Therefore, in this study, we assessed the OIM potential of such patterns. Towards this aim, we first established a direct co-culture model and used it to investigate the interactions between murine M1 macrophages (J774.A1) and murine preosteoblasts (MC3T3-E1) at various cell ratios and over different culturing times. The direct co-culture model was then applied to study the effects of 3D printed submicron pillars on both types of cells.

2. Materials and methods

2.1. Cell preculture

2.1.1. Macrophages preculture and polarization

Murine macrophages (J774A.1, passage 15, Merck KGaA, Germany) were incubated in 25 cm^2 flasks (1×10^4 cells/cm^2) (Greiner Bio-One GmbH, Austria) containing 10 mL Dulbecco's Modified Eagle's medium (DMEM), 10 % (v/v) fetal bovine serum (FBS) and 1 % penicillin-streptomycin (pen-strep) (ThermoFisher Scientific, US). The culture medium was refreshed every 2–3 days until the cells reached confluency. Confluent cells, at a density of approximately 1×10^5 cells/cm^2, were stimulated towards the M1s by the addition of 100 ng/mL LPS (Sigma-Aldrich, Germany) and 10 ng/mL IFN-γ (Sigma-Aldrich, Germany) for 3 days [22]. Polarization towards M2s was stimulated by adding 10 ng/mL interleukin-4 (IL-4) (Sigma-Aldrich, Germany) for 3 days [22]. Next, (non)polarized macrophages were scraped and seeded alone or with OBs on the substrates. Day 3 of M1 polarization is considered as day 0 in experiments that the M1 cells co-cultured with osteoblasts. Unstimulated macrophages (M0) (Fig. 1a) were used as a control group.

2.1.2. Preosteoblasts preculture

Murine preosteoblasts MC3T3-E1 (OBs) (passage 13) were incubated in a 25 cm^2 culture flask (5×10^3 cells/cm^2) in alpha Minimum Essential Medium (αMEM; ThermoFisher Scientific, US) without ascorbic acid but supplemented with 10 % FBS and 1 % pen-strep. The culture medium was changed every 2–3 days until confluency was reached. Next, the OBs were trypsinized and seeded alone or with macrophages subsets (Table 1).

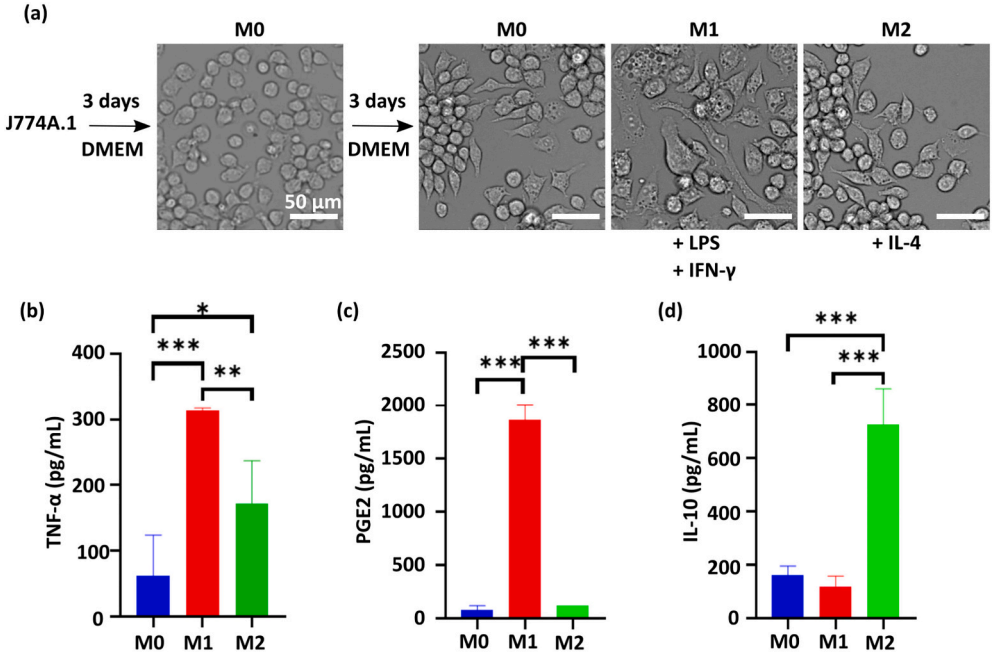

Fig. 1. Characterization of macrophages on day 0: (a) morphology of the M0, M1-stimulated and M2-stimulated macrophages. Expression of (b) TNF-α, (c) PGE2, and (d) IL-10 by the M0, M1 and M2 macrophages (* $p < 0.05$, ** $p < 0.01$, *** $p < 0.001$).

Table 1
The density of M1 and OB cells in the direct co-culture model.

Groups	M1 density (#/cm^2)	OB density (#/cm^2)
M1	5×10^3	–
OB	–	5×10^3
CO11	5×10^3	5×10^3
CO12	1×10^4	5×10^3

2.2. Direct co-culture of macrophages and OBs

Co-cultures of OBs and M1s at the ratio of 1:1 (CO11) and at the ratio of 1:2 (CO12) were studied in a direct co-culture system (Table 1). For CO11 co-cultures, 5×10^3 cells/cm^2 of OBs were mixed with 5×10^3 cells/cm^2 M1s and seeded simultaneously in a 48-well plate in mixed medium (αMEM: DMEM (1:1), 10 % FBS, and 1 % pen-strep). The cells were incubated at 37 °C and 5 % CO_2. For the CO12 co-cultures, 5×10^3 cells/cm^2 OBs were mixed with 1×10^4 cells/cm^2 M1s and were cultured in αMEM:DMEM (1:1) under similar conditions. As controls, M0s, M1s, M2s, and OBs (5×10^3 cells/cm^2) were seeded in the mixed medium. After 2 days, the mixed medium was supplemented with 50 μg/mL ascorbic acid (AA; Sigma-Aldrich, Germany) and 4 mM β-glycerolphosphate (β-GL; Sigma-Aldrich, Germany) to induce osteogenic differentiation. The culture medium was refreshed every 2–3 days until day 14.

2.3. Direct co-culture of M1s and OBs on the patterned surfaces

2.3.1. 3D printing of submicron pillars

A Nanoscribe Photonic Professional GT laser lithography system (Nanoscribe, Germany) working on the basis of two-photon polymerization was used to fabricate the patterns. The general writing language (GWL) file of the designed pillars (diameter = 300 nm, height = 500 nm, and interspacing = 700 nm) was prepared as previously described [19,23,24]. A curable acrylate-based photosensitive resin, namely IP-L780, was polymerized under the exposure of an infrared laser beam, and submicron pillars were fabricated using a previously described protocol [22]. After polymerization, the samples were immersed in propylene glycol monomethyl ether acetate (PGMEA) (Sigma-Aldrich, Germany) for 25 min followed by 5 min rinsing with isopropyl alcohol (IPA) (Sigma-Aldrich, Germany) and blow-drying with air.

The morphology of the pillars was characterized by scanning electron microscopy (SEM) (Helios Nano Lab 650, FEI, USA). A gold-coater (JFC-1300, JEOL, Japan) was used to sputter-coat a thin layer of gold (layer thickness ≈ 5 nm) on the specimens prior to imaging. The images of the samples were acquired at a tilt angle of 30°.

2.3.2. Cell seeding on the submicron pillars

The patterned samples were disinfected with 70 % ethanol (Sigma-Aldrich, Germany) followed by rinsing twice with phosphate-buffered saline (PBS) (ThermoFisher Scientific, US). OBs and CO12 co-cultures were prepared as described above and were seeded on the sterile patterned substrates (referred to as OBp and CO12p hereafter) and non-patterned control surfaces (referred to as OB and CO12 hereafter). In the mono-cultures, 5×10^3 cells/cm^2 of OBs were seeded on the patterned and control surfaces. In the co-cultures, 5×10^3 cells/cm^2 OBs and 1×10^4 cells/cm^2 M1s were seeded on the specimens. A mixed medium of αMEM:DMEM (1:1, supplemented with AA and β-GL) was used, which was refreshed every 2–3 days.

2.4. Cytokine profiles

The secretion of cytokines by the macrophages (M0s, M1s, and M2s) in response to the stimulating factors and preosteoblast cells was measured using a VICTOR X3 Multimode Plate Reader (PerkinElmer, Groningen, The Netherlands) on days 0, 1, 3, and 7. The expression of TNF-α, IL-10, and PGE2 in the supernatant of cells was measured by enzyme-linked immunosorbent assay (ELISA) following the manufacturer's instructions (Abcam, UK). A mixed culture medium was used as a control. Each experimental condition was repeated 4 times (n = 4).

2.5. Cells viability

The viability of cells in both mono and co-culture conditions was assessed by a LIVE/DEAD™ Viability/Cytotoxicity Kit (ThermoFisher Scientific, US) on days 3, 7, 10, and 14. In short, 48-well plates containing mono- and co-culture cells were retrieved from the incubator and were washed with 1× PBS. Next, a live/dead solution of 2 μM calcein acetoxymethyl ester (calcein AM) and 3 μM ethidium homodimer (EthD) diluted in PBS was added to the OB, CO11, and CO12 cultures. For M0s, M1s, and M2s, a live/dead solution of 0.8 μM calcein AM and 3 μM EthD was used. The samples were placed in the incubator for 30 min. Subsequently, the solution was discarded and replaced by 1× PBS. Fluorescent images were taken with a ZOE Fluorescent Cell Imager (BioRad, US) at 5 random locations. For each condition, four different samples were analyzed (n = 4).

2.6. Osteogenic and mineralization markers

2.6.1. RUNX2 staining

The effects of the M1 cells and patterned surfaces on the osteogenic differentiation of the preosteoblasts were assessed using Runt-related transcription factor (RUNX2) and ALP assays. For RUNX2, the cells were washed twice with 1× PBS and were fixed with 4 % paraformaldehyde (PFA; Sigma-Aldrich, Germany) for 15 min at room temperature. After rinsing twice with 1× PBS, the cells were permeabilized with 0.5 % Triton/PBS (Sigma-Aldrich, Germany) for 5 min at 4 °C followed by blocking with 1 % bovine serum albumin in PBS (BSA/PBS; Sigma-Aldrich, Germany) for 5 min at 37 °C. Primary rabbit RUNX2 antibody (Abcam, UK) was diluted in BSA/PBS (1:250) and was added to the wells. After 1 h incubation at 37 °C, the cells were rinsed 3 times with 0.5 % Tween/PBS (Sigma-Aldrich, Germany). Alexa 488 donkey anti-rabbit (ThermoFisher Scientific, US) was added to the wells as a secondary antibody in 1 % BSA/PBS (1:200), which were then incubated for 1 h at room temperature. Subsequently, the cells were washed 3 times with 0.5 % Tween/PBS (Sigma-Aldrich, Germany) and once with 1× PBS. The specimens were mounted on a glass slide using Prolong gold antifade reagent (containing 4′,6-diamidino-2-phenylindole (DAPI), ThermoFisher Scientific, US). Fluorescent images were taken using a ZOE Fluorescent Cell Imager (BioRad, US) at 5 random locations of each sample. For each condition, two different specimens were analyzed (n = 2).

2.6.2. ALP activity

The analysis was performed according to the manufacturer's instruction kit (ALP Assay Fluorometric kit, Abcam, UK). Briefly, 100 μL culture supernatant was collected on days 7, 11, 14, 21, and 28 and was added to a 96-well plate (n = 4/group). The mixed medium was considered as a control sample. Next, 20 μL of the ALP enzyme solution was added to the standard wells; 20 μL of the ALP reaction mixture (2 μL of 5 mM non-fluorescent 4-methylumbelliferyl phosphate disodium salt (4-MUP) + 18 μL ALP assay buffer) was added to the specimens followed by incubation for 30 min at 25 °C. Next, the stop solution was added to all the samples. After thorough mixing, the fluorescent absorbance was read (E_x/E_m = 360/440 nm) using a VICTOR X3 multimode plate reader (PerkinElmer, Groningen, The Netherlands).

2.6.3. Alizarin red staining (ARS)

After 28 days of culture, the samples were washed twice with 1× PBS and were fixed with 4 % paraformaldehyde (PFA; Sigma-Aldrich, Germany) for 15 min at room temperature. Next, the cells were washed twice with distilled water. A 2 % ARS/PBS (Sigma-Aldrich, Germany)

solution was added to the specimens, which were then shaken with a thermal shake Lite plate shaker (VWR, USA) at 300 rpm for 20 min. Next, the cells were washed 5 times with distilled water on a plate shaker at 300 rpm for 5 min. The specimens were then dried at room temperature and were imaged with a WIFI digital microscope (Rotek, China) at five random locations for each specimen. The average mineralized area (%) was reported (n = 4).

2.7. Image analysis

Image processing was performed using the open-source software FIJI (https://imagej.net/software/fiji/downloads). For counting live and dead cells, the living cells were selected by thresholding the green fluorescent images. The threshold was altered to fit all the green-stained cells present. The remaining part of the image was then segmented using the "watershed" function. Finally, all the particles bigger than the smallest cell present in the image were counted. The dead cells were counted by applying the same method to the red fluorescent images.

RUNX2 expression was quantified as the sum of the green fluorescence intensity in the cells present in a fixed area (234.4 × 234.4 μm^2). Firstly, the cells were selected using the same thresholding method as the one applied to the live/dead images. Secondly, the intensity of the green marker was measured within each cell. Finally, the results of all the cells were summed up to obtain the total amount of RUNX2 expression in the area. The mean and standard deviation (SD) of the 5 random images were included in the graph. For all the images, the background noise was measured as well. The mean value of the background noise was subsequently subtracted from the measured values. In order to quantify the mineralized area, the bright-field images were color thresholded in Fiji (HUE = 0–30, Saturation, 0–255, Brightness

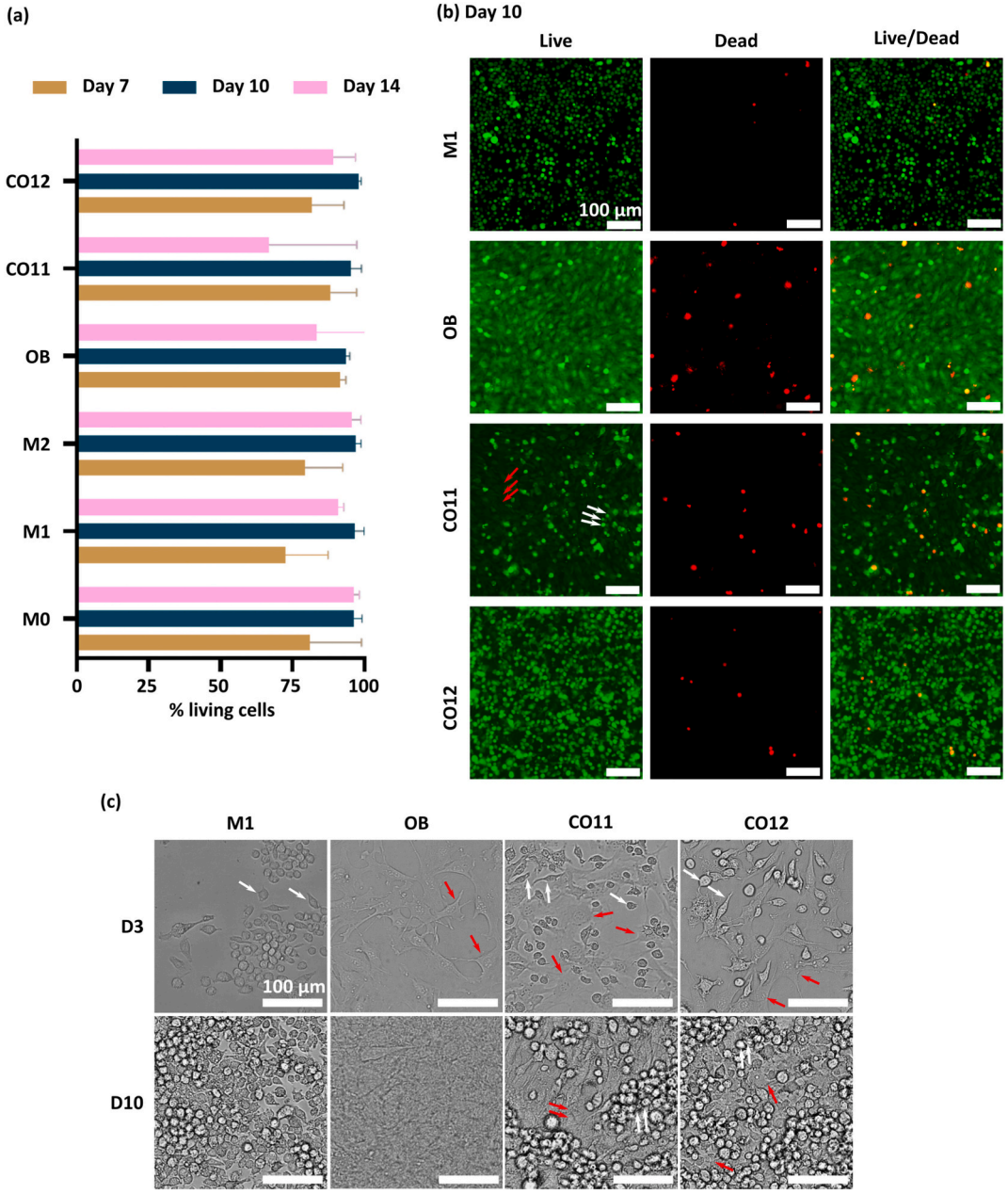

Fig. 2. Cell viability and growth in the mono- and direct co-cultures. (a) percentage of living cells on days 7, 10, and 14. (b) Live/dead staining of M1s and OBs in the mono and co-cultures (CO11 and CO12) after 10 days of culture. (c) Spatial distribution of OBs and M1s after 3 and 10 days of culture. White and red arrows indicate M1 and OB cells, respectively (* $p < 0.05$, ** $p < 0.01$, *** $p < 0.001$).

0–255).

2.8. Statistical analysis

Data are reported as mean ± (SD). One-way ANOVA using the Sidak's multiple comparisons test was performed in GraphPad Prism version 8.0.1 for Windows (GraphPad Software, USA) to analyze the differences between mono- and co-cultures. For the tests with multiple conditions at multiple days, two-way ANOVA was used followed by the Sidak's multiple comparisons test. Probability values <0.05 were considered statistically significant. The outliers in the ELISA results were removed using the ROUT test with Q = 1 %.

3. Results and discussion

3.1. Macrophage activation

After 3 days of macrophage polarization, elongated and flatter morphologies were mainly observed for the M1 cells while the M2 cells were less polarized (Fig. 1a). Similar morphologies of activated cells have been observed before [22,25]. The expressions of TNF-α, PGE2, and IL-10 were measured in the (non)activated macrophages. The M1 cells expressed significantly higher levels of TNF-α and PGE2, confirming the pro-inflammatory phenotype of the M1 cells (Fig. 1b,c) [26]. As expected, IL-10 was predominantly expressed in the M2 cells, which is in agreement with their prohealing state (Fig. 1d) [27].

3.2. Direct co-culture of M1 macrophages and MC3T3-E1 cells

The viability of M0, M1, M2, and OB in mono-culture and of the OB-M1 in co-cultures (OB:M1 = 1:1 & 1:2) was very high and constant during the entire 14-days period of incubation, indicating that the proposed mixed culture medium (*i.e.,* αMEM:DMEM, 1:1) provided the needed nutrients for both cell types (Fig. 2a, b). Finding a suitable culture medium is essential in the direct co-culture models. Depending on the type, origin, and ratio of the (pre)osteoblasts and macrophages, different types of media have been used in previous studies [15,28,29]. For example, a mixture of α-MEM and RPMI 1640 (Roswell Park Memorial Institute medium) (ratio 1:1) was applied for the direct co-culture of MC3T3-E1 preosteoblasts and murine bone marrow M1, followed by IL-4 treatment [15,29]. On the other hand, in indirect co-cultures, the conditioned medium of the macrophages seeded on the biomaterials was used to analyze its effect on bone cells [30]. However, reproducing the desired level of cytokines in the conditioned medium is problematic at the first step. It requires further dilution with a medium suitable for other cell types at the second step, leading to a prolonged *in vitro* procedure [1]. On the other hand, the advantage of an indirect model is the flexibility it offers regarding the origin of preosteoblasts and immune cells. By comparison, cells should be from the same species in direct co-cultures to prevent unwanted immune reactions that are caused by xenogenic cells [31].

After 3 days in mono-cultures, the preosteoblasts adopted a fully spread morphology whereas the M1 cells seemed to show a mixture of M1 and M2 morphologies in their colonies (Fig. 2c). In the co-cultures (CO11 and CO12), the preosteoblasts and the macrophages were clearly distinguishable and seemed to nicely co-exist. Both M1- and M2-like morphologies were observed with macrophages appearing smaller and thicker than the preosteoblasts (Fig. 2c). After 10 days of culture, thick and dense layers of cells were visible in all the cultures. The macrophages formed clusters of cells. In the co-cultures, they were present mostly on top of the preosteoblast cell layer. These findings are in agreement with the live/dead results, indicating the ability of both cell types to proliferate in the co-culture conditions of this study.

Due to the different types of macrophage morphology observed and the high cell density, recognizing the dominant phenotype of macrophages was not feasible. Therefore, we further analyzed the inflammatory cytokines in the culture media.

3.2.1. Inflammatory response

The pro- and anti-inflammatory cytokines secreted in the mono- and co-cultures were measured to determine whether the M1 macrophages retained their phenotype. At 1 and 3 days after seeding, the expression of TNF-α was similar in mono- and co-cultures (Fig. 3a), which was threefold lower than the amount of TNF-α expressed by M1 cells on day 0 (*i.e.*, day 3 of M1 polarization presented in Fig. 1b). Furthermore, the amounts of IL-10 expressed on days 1 and 3 (Fig. 3b) in all culture conditions were comparable with the levels produced by M0 cells on day 0 (Fig. 1d), suggesting that M1 cells switched their phenotype to M0 during the first 3 days of culture. This transition from M1 to M0 phenotype that was observed in both the mono- and co-culture conditions may be related to the mechanical (scraping) stress that the cells experienced during the harvesting procedure [32]. To maintain the phenotypic stability of cells, the presence of polarization stimuli is required [27,32]. There is little information on the way OBs modulates the immune cells. Interestingly here, after 7 days of seeding, we observed a significant increase in the expression of TNF-α in mono- and co-cultures as compared to days 1 and 3 (Fig. 3a), verifying the continued M1 phenotype. The highest level of TNF-α was observed in the co-cultures (CO11, CO12), meaning that not only M1 cells but also OBs contributed to the enhanced inflammation. This was not observed in an indirect co-culture model (Fig. S1, supplementary information) where the TNF-a levels after 3 days were comparable with the M1 mono-culture, showing that the direct contact between M1s and OBs affects the inflammatory microenvironment with consequences on the differentiation of OBs. The concentration of IL-10 did not change during the first 7 days of culture, confirming the inflammatory conditions in co-cultures. Here, the expression of PGE2, a bone resorption marker, in OBs increased in the pro-inflammatory environment of day 7 (Fig. 3c, a). The amount of PGE2 released in the mono-culture was highest on day 1 and then significantly dropped over time (Fig. 3c). While the level of PGE2 in the co-culture (CO11, CO12) was high on day 1, it dropped on day 3 but then rose again on day 7 (Fig. 3c). The high level of PGE2 on day 1 was most likely caused by the trypsinization of OBs before seeding, which could quickly stimulate the synthesis of PGE2 [33]. While on day 7, high TNF-α concentration on co-cultures activated mediators to enhance the expression of PGE2 in OBs. Previous studies have also found a direct influence of TNF-α on the secretion of PGE2 in osteoblasts in indirect co-cultures [6,26]. Although inflammatory cytokines are primarily expressed by M1 cells, bone cells (*e.g.*, OBs and MSCs) are known to produce pro-inflammatory cytokines too. OBs, hMSCs, and chondrocytes produce IL-6, which has been reported to promote bone resorption in response to IL-1 and TNF-α both *in vitro* [34,35] and *in vivo* [36]. It should be noted that MSCs are considered the regulator of inflammation at the very early stages (*i.e.*, after 3 days) [37,38]. MSCs are activated in response to inflammation, convert pro-inflammatory macrophages to anti-inflammatory ones, and reduce the inflammation through the expression of PGE2 *via* the COX2 signaling pathway [38]. Here, the expression of PGE2 in OBs increased in the pro-inflammatory environment of day 7 (Fig. 3c, a).

3.2.2. Osteogenic response

We assessed the impact of inflammatory cells on the osteogenic activity of preosteoblasts. On day 7 after seeding, the expression of RUNX2 in the mono-culture of OBs was two times higher than the one expressed in the co-culture CO12 (Fig. 3d), indicating that the inflammatory M1 cells attenuated the differentiation of preosteoblasts. The ALP activity of OBs on days 21 and 28 was significantly higher than the level of ALP secretion in the co-cultures (Fig. 3f). In contrast, the ALP activity of preosteoblasts on days 7 and 11, was similar in both mono- and co-cultures (Fig. 3f). Furthermore, preosteoblasts deposited a higher amount of calcium in the mono-culture (Fig. 3g). The reduced matrix mineralization in the co-cultures can be explained by the increased

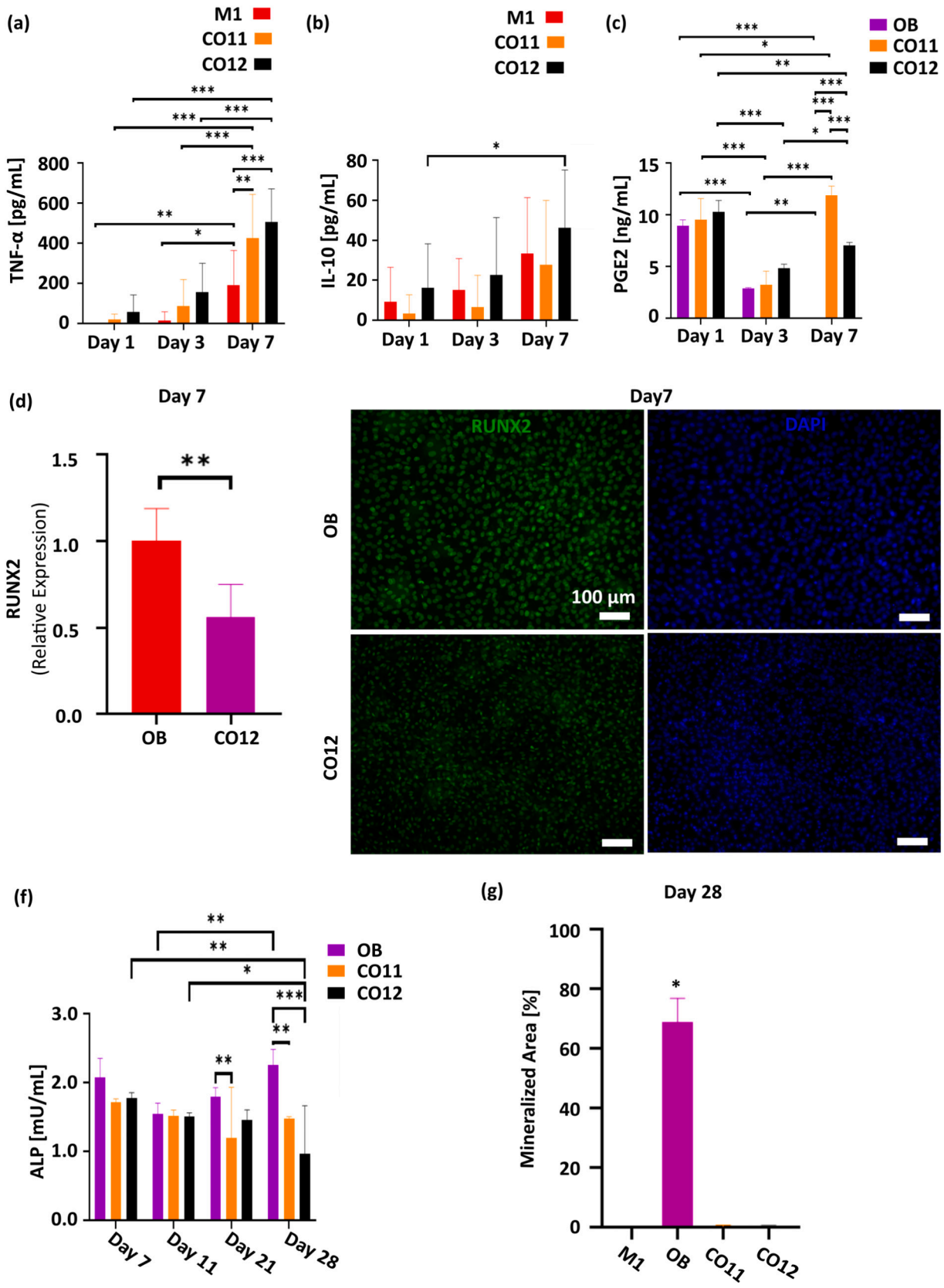

Fig. 3. (a) Secretion of pro-inflammatory, TNF-α, (b) anti-inflammatory cytokine, IL10, and (c) PGE2 after 1, 3, and 7 days of co-culturing OBs with M1s. (d) The expression level of RUNX2, (e) the immunostaining of nuclei and RUNX2 differentiation marker in OBs co-cultured with M1s. The expression level is normalized with respect to the level of expression of RUNX2 in preosteoblasts in the mono-culture. (f) ALP activity and (g) mineralization of preosteoblasts (ARS) in mono- and co-cultures over a culture period of 28 days (* $p < 0.05$, ** $p < 0.01$, *** $p < 0.001$).

secretion of TNF-α and PGE2 after 7 days of culture. The effect of PGE2 on the activity of preosteoblasts is dependent on the concentration of TNF-α [3,26]. At high TNF-α concentrations (*i.e.*, pro-inflammatory conditions), PGE2 stimulates the activity of osteoclasts, whereas in the presence of low concentrations of inflammatory cytokines, PGE2 enhances the proliferation of osteoblasts [3,26]. Ideally, an M1-to-M2 polarization will shift high TNF-α towards low concentrations. Enhanced osteogenic activity is expected to follow. However, we did not observe the M1-to-M2 transition in co-cultured samples. Prolonged inflammatory response, therefore, adversely affected osteogenesis in CO11 and CO12. The addition of exogenous growth factors to the culture media may promote OIM [39,40]. In the presence of biomaterials, surface modification may help in modulating the response of macrophages and osteoblasts [13,41].

3.2.3. *Modulation of OIM response via submicron pillars*

We further investigated the influence of specific physical patterns on the response of both types of cells in the direct co-culture model established above. In our previous studies, we have extensively examined the effects of the spatial arrangement of submicron pillars on preosteoblasts [23] and macrophages [22]. Here, we studied whether submicron pillars can modulate the pro-inflammatory response observed in the co-culture towards stimulating the osteogenic response. Therefore, the growth of both cell types (CO12) on the patterned surfaces was assessed (Fig. 4a). On day 3 of culture, both macrophages and preosteoblasts were observed on the patterned area (CO12p). M1 macrophages in the co-culture tended to migrate to the patterned surface. On day 7 of culture, a monolayer of preosteoblasts covered the patterned area and the macrophages, with a dominant round morphology (indicative of the M2 phenotype [22]), were located on top of the preosteoblast layer. The level of RUNX2 expression on day 7 was significantly upregulated on the submicron patterned surface as compared with the flat control (Fig. 4b, c), indicating the potential of such nano-engineered surfaces to promote the differentiation of preosteoblast in inflammatory conditions possibly enabled through M1-to-M2 switching. In our previous studies with mono-cultures, this particular design of submicron pillars was observed to promote the matrix mineralization by preosteoblasts [23] and the prohealing response of macrophages [22]. In the direct co-culture model used in this study, the pillars may have played a similar role, effectively activating the anti-inflammatory state, and enhancing the differentiation of preosteoblasts. Nevertheless, the underlying mechanism involved is yet to be established.

The main signaling pathway revealed so far in OIM biomaterials is the TLR4-NF-κB pathway, in which toll-like receptor 4 (TLR-4) identifies the biomaterials and NF-κB regulates the inflammation and improves bone regeneration [42]. In the mono-cultures, titania nanotubes (diameter ~ 78 nm) suppressed the NF-κB pathway and reduced the inflammation in M1 macrophages (RAW 264.7) [43]. When

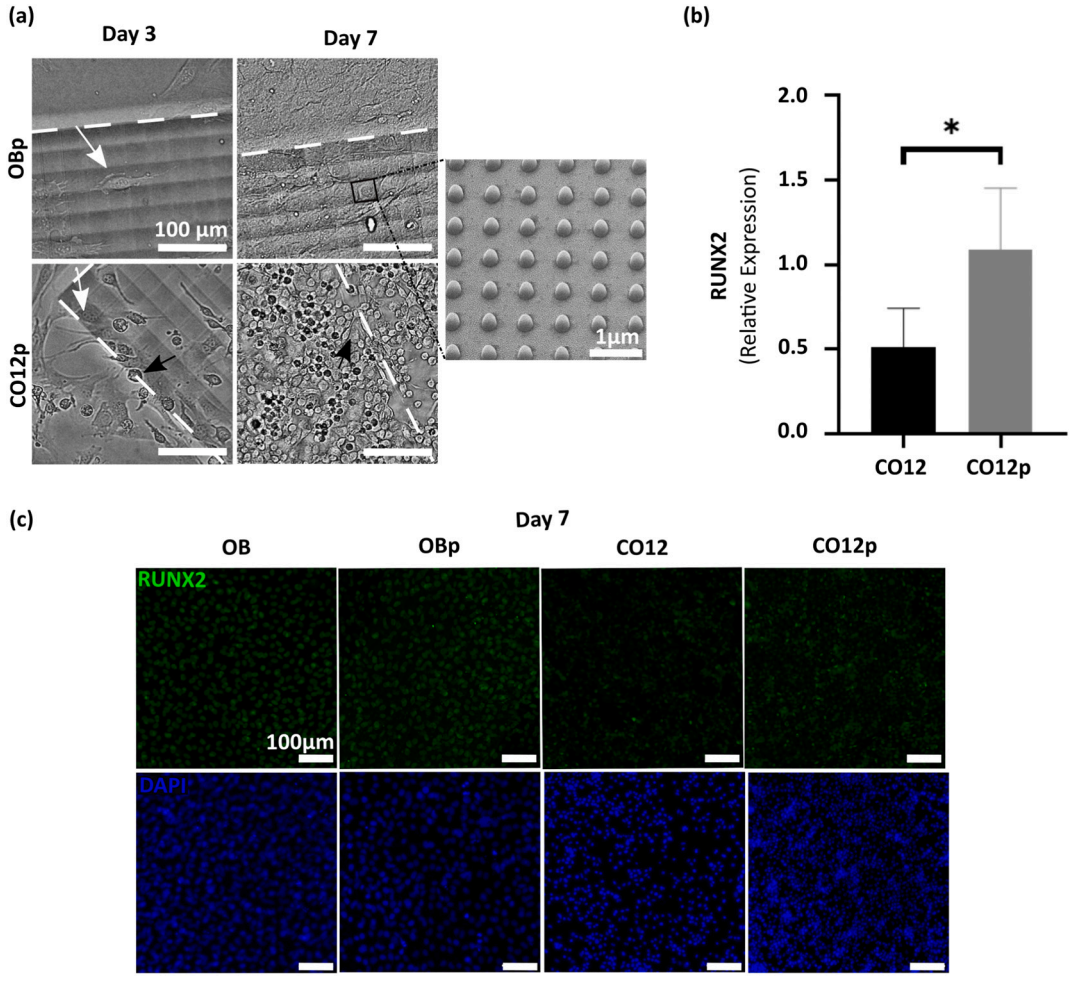

Fig. 4. (a) Interactions of OBs and M1s in the mono- and direct co-cultures on the patterned and non-patterned substrates. Black and white arrows indicate M1s and OBs, respectively. The dotted lines indicate the edge between the patterned and non-patterned area. (b) The expression of RUNX2 in the OBs co-cultured with M1s on the non-patterned (CO12) *vs.* patterned (CO12p) surfaces. The expression level is normalized with respect to the level of expression of RUNX2 in preosteoblasts in the mono-culture. (c) Immunostained images of nuclei and RUNX2 expressed in the mono- and co-cultures on the patterned and non-patterned substrates (* $p < 0.05$, ** $p < 0.01$, *** $p < 0.001$).

macrophages (RAW 264.7) were co-cultured with MSCs (in transwells), titania nanotubes with a diameter of 110 nm activated the NF-κB pathway, leading to high inflammation [44]. As a result, MSCs were actively engaged in stimulating prohealing response, leading to higher matrix mineralization and ALP activity than nanotubes of 30 nm and 70 nm diameter [44].

To date, the research on osteoimmunomodulatory biomaterials has been predominantly performed using indirect *in vitro* co-cultures models. This type of model facilitates assessing the paracrine effects of different cell types while neglecting the effects of direct cell-cell contact. Using such indirect models, it has been found that while nano-engineered topographies may promote the expression of osteogenic factors (such as BMP2/6) in macrophages, the resulting conditioned medium containing higher BMPs does not necessarily stimulate the mineralization of bone marrow-derived mesenchymal stem cells (BMSCs) [16]. Another approach for indirect co-culturing of bone and immune cells utilizes transwell systems that enable the co-culturing of two cell types by separating them *via* a membrane [13]. BMSCs seeded on titania nanowires in transwells have been found to decrease the level of inflammatory cytokines and polarize the M1 macrophages towards an M2 prohealing phenotype [13]. The titania nanowires were found to activate the ROCK-mediated cyclooxygenase-2 (COX2) pathway that modulates the secretion of PGE2, thereby enhancing the osteogenic activity of the BMSCs [13].

Despite the complexity of direct co-culture models, they are essential to closely mimic the *in vivo* conditions as closely as possible [16]. Furthermore, although mono-cultures and indirect co-culture models can reveal the signaling pathways behind cell-biomaterial interactions [13], the direct interactions between different cell types and the biomaterials should be assessed in such direct *in vitro* models to improve the design of biomaterials for *in vivo* studies.

4. Conclusions

We developed a direct co-culture model incorporating bone and inflammatory cells to more closely mimic the interaction of those cell types *in vivo*. The spatial distribution of both cell types was homogenous until day 3, while from day 7 a layered distribution was observed with preosteoblasts occupying the space underneath the macrophages. Although preosteoblasts were cultured with inflammatory M1 cells, we barely observed inflammatory cytokines in the co-culture microenvironment up until day 7, indicating the switch in polarization state from M1 to M0. On day 7, the high level of PGE2 in the inflammatory condition attenuated the preosteoblast differentiation, as revealed by a lower level of RUNX2 measured in the co-cultures as compared to the mono-culture. Consequently, the ALP activity and mineralization of preosteoblast decreased on day 28 of co-culture. Interestingly, the integration of submicron pillars in the co-culture system enhanced the differentiation of preosteoblasts, indicating the osteoimmunomodulatory potential of such surface patterns.

CRediT authorship contribution statement

A.A. Zadpoor: Conceptualization, Resources, Writing - Review & Editing, Supervision, Funding acquisition, Project administration, Methodology.

L.E. Fratila-Apachitei: Conceptualization, Resources, Writing - Review & Editing, Supervision, Project administration, Methodology.

M. Minneboo: Validation, Writing - Review & Editing.

B.I.M. Eijkel: Validation, Formal analysis, Investigation, Data Curation, Methodology, Writing-Review & Editing, Visualization, Software.

M. Nouri-Goushki: Conceptualization, Formal analysis, Investigation, Data Curation, Methodology, Writing- Original Draft, Visualization.

Data availability

The raw/processed data required to reproduce these findings cannot be shared at this time as the data also forms part of an ongoing study.

Declaration of competing interest

The authors declare that they have no known competing financial interests or personal relationships that could have appeared to influence the work reported in this paper.

Acknowledgments

The research leading to these results has received funding from the European Research Council under the ERC grant agreement no [677575]. We would like to thank Prof. dr. Urs Staufer (Department of Precision and Microsystems Engineering, TU Delft) for the access to the Nanoscribe equipment, and Dr. Cornelis W. Hagen (Department of Imaging Physics, TU Delft) for the access to the SEM equipment.

Appendix A. Supplementary data

The following PDF file is available free of charge: the file includes an indirect study of inflammatory M1 macrophages with preosteoblast cells. Supplementary data to this article can be found online at https://doi.org/10.1016/j.bioadv.2022.212993.

References

[1] G. Mestres, S.-S.D. Carter, N.P. Hailer, A. Diez-Escudero, A practical guide for evaluating the osteoimmunomodulatory properties of biomaterials, Acta Biomater. 130 (2021) 115–137.
[2] H. Takayanagi, Osteoimmunology: shared mechanisms and crosstalk between the immune and bone systems, Nat. Rev. Immunol. 7 (4) (2007) 292–304.
[3] J.M. Curran, J.A. Gallagher, J.A. Hunt, The inflammatory potential of biphasic calcium phosphate granules in osteoblast/macrophage co-culture, Biomaterials 26 (26) (2005) 5313–5320.
[4] L. Gilbert, X. He, P. Farmer, S. Boden, M. Kozlowski, J. Rubin, M.S. Nanes, Inhibition of osteoblast differentiation by tumor necrosis factor-α, Endocrinology 141 (11) (2000) 3956–3964.
[5] M. Feldmann, R.N. Maini, Anti-TNF therapy, from rationale to standard of care: what lessons has it taught us? J. Immunol. 185 (2) (2010) 791–794.
[6] J.B. Gonzales, M.A. Purdon, S.M. Horowitz, In vitro studies on the role of titanium in aseptic loosening, Clin. Orthop. Relat. Res. (1996) 330.
[7] K. Hess, A. Ushmorov, J. Fiedler, R.E. Brenner, T. Wirth, TNFα promotes osteogenic differentiation of human mesenchymal stem cells by triggering the NF-κB signaling pathway, Bone 45 (2) (2009) 367–376.
[8] L. Rifas, T-cell cytokine induction of BMP-2 regulates human mesenchymal stromal cell differentiation and mineralization, J. Cell. Biochem. 98 (4) (2006) 706–714.
[9] J. Ding, O. Ghali, P. Lencel, O. Broux, C. Chauveau, J.C. Devedjian, P. Hardouin, D. Magne, TNF-α and IL-1β inhibit RUNX2 and collagen expression but increase alkaline phosphatase activity and mineralization in human mesenchymal stem cells, Life Sci. 84 (15) (2009) 499–504.
[10] Y. Xie, C. Hu, Y. Feng, D. Li, T. Ai, Y. Huang, X. Chen, L. Huang, J. Tan, Osteoimmunomodulatory effects of biomaterial modification strategies on macrophage polarization and bone regeneration, Regen. Biomater. 7 (3) (2020) 233–245.
[11] K. Sakthivel, A. O'Brien, K. Kim, M. Hoorfar, Microfluidic analysis of heterotypic cellular interactions: a review of techniques and applications, TrAC Trends Anal. Chem. 117 (2019) 166–185.
[12] L. Saldaña, F. Bensiamar, G. Vallés, F.J. Mancebo, E. García-Rey, N. Vilaboa, Immunoregulatory potential of mesenchymal stem cells following activation by macrophage-derived soluble factors, Stem Cell Res Ther 10 (1) (2019) 58.
[13] K. Li, S. Liu, T. Hu, I. Razanau, X. Wu, H. Ao, L. Huang, Y. Xie, X. Zheng, Optimized nanointerface engineering of micro/nanostructured titanium implants to enhance cell-nanotopography interactions and osseointegration, ACS Biomater Sci. Eng. 6 (2) (2020) 969–983.
[14] M.D. Swartzlander, A.K. Blakney, L.D. Amer, K.D. Hankenson, T.R. Kyriakides, S. J. Bryant, Immunomodulation by mesenchymal stem cells combats the foreign body response to cell-laden synthetic hydrogels, Biomaterials 41 (2015) 79–88.
[15] L.A. Córdova, F. Loi, T.-H. Lin, E. Gibon, J. Pajarinen, A. Nabeshima, L. Lu, Z. Yao, S.B. Goodman, CCL2, CCL5, and IGF-1 participate in the immunomodulation of osteogenesis during M1/M2 transition in vitro, J. Biomed. Mater. Res. A 105 (11) (2017) 3069–3076.
[16] Z. Chen, A. Bachhuka, S. Han, F. Wei, S. Lu, R.M. Visalakshan, K. Vasilev, Y. Xiao, Correction to "Tuning chemistry and topography of nanoengineered surfaces to

manipulate immune response for bone regeneration applications", ACS Nano 13 (3) (2019), 3739-3739.
[17] D. Naskar, S. Nayak, T. Dey, S.C. Kundu, Non-mulberry silk fibroin influence osteogenesis and osteoblast-macrophage cross talk on titanium based surface, Sci. Rep. 4 (1) (2014) 4745.
[18] G. Vallés, F. Bensiamar, L. Crespo, M. Arruebo, N. Vilaboa, L. Saldaña, Topographical cues regulate the crosstalk between MSCs and macrophages, Biomaterials 37 (2015) 124–133.
[19] M. Nouri-Goushki, M.J. Mirzaali, L. Angeloni, D. Fan, M. Minneboo, M. K. Ghatkesar, U. Staufer, L.E. Fratila-Apachitei, A.A. Zadpoor, 3D printing of large areas of highly ordered submicron patterns for modulating cell behavior, ACS Appl. Mater. Interfaces 12 (1) (2020) 200–208.
[20] M. Nouri-Goushki, A. Isaakidou, B.I.M. Eijkel, M. Minneboo, Q. Liu, P.E. Boukany, M.J. Mirzaali, L.E. Fratila-Apachitei, A.A. Zadpoor, 3D printed submicron patterns orchestrate the response of macrophages, Nanoscale 13 (2021) 14304–14315.
[21] M. Nouri-Goushki, L. Angeloni, K. Modaresifar, M. Minneboo, P.E. Boukany, M. J. Mirzaali, M.K. Ghatkesar, L.E. Fratila-Apachitei, A.A. Zadpoor, 3D-printed submicron patterns reveal the interrelation between cell adhesion, cell mechanics, and osteogenesis, ACS Appl. Mater. Interfaces 13 (29) (2021) 33767–33781.
[22] M. Nouri-Goushki, A. Isaakidou, B. Eijkel, M. Minneboo, Q. Liu, P. Boukany, M. Mirzaali, L. Fratila-Apachitei, A. Zadpoor, 3D printed submicron patterns orchestrate the response of macrophages, Nanoscale 13 (34) (2021) 14304–14315.
[23] M. Nouri-Goushki, L. Angeloni, K. Modaresifar, M. Minneboo, P.E. Boukany, M. J. Mirzaali, M.K. Ghatkesar, L.E. Fratila-Apachitei, A.A. Zadpoor, 3D printed submicron patterns reveal the interrelation between cell adhesion, cell mechanics, and osteogenesis, ACS Appl. Mater. Interfaces 13 (29) (2021) 33767–33781.
[24] M. Nouri-Goushki, A. Sharma, L. Sasso, S. Zhang, B.C. Van der Eerden, U. Staufer, L.E. Fratila-Apachitei, A.A. Zadpoor, Submicron patterns-on-a-chip: fabrication of a microfluidic device incorporating 3D printed surface ornaments, ACS Biomater Sci. Eng. 5 (11) (2019) 6127–6136.
[25] T.J. Bartosh, J.H. Ylostalo, Macrophage inflammatory assay, Bio-Protoc. 4 (14) (2014), e1180.
[26] C.-W. Wei, J.-Y. Cheng, T.-H. Young, Elucidating in vitro cell-cell interaction using a microfluidic coculture system, Biomed. Microdevices 8 (1) (2006) 65–71.
[27] F. Loi, L.A. Córdova, J. Pajarinen, T.-H. Lin, Z. Yao, S.B. Goodman, Inflammation, fracture and bone repair, Bone 86 (2016) 119–130.
[28] J. Pajarinen, Y. Tamaki, J.K. Antonios, T.-H. Lin, T. Sato, Z. Yao, M. Takagi, Y. T. Konttinen, S.B. Goodman, Modulation of mouse macrophage polarization in vitro using IL-4 delivery by osmotic pumps, J. Biomed. Mater. Res. A 103 (4) (2015) 1339–1345.
[29] F. Loi, L.A. Córdova, R. Zhang, J. Pajarinen, T.-H. Lin, S.B. Goodman, Z. Yao, The effects of immunomodulation by macrophage subsets on osteogenesis in vitro, Stem Cell Res Ther 7 (1) (2016) 15.
[30] C. Li, L. Yang, X. Ren, M. Lin, X. Jiang, D. Shen, T. Xu, J. Ren, L. Huang, W. Qing, J. Zheng, Y. Mu, Groove structure of porous hydroxyapatite scaffolds (HAS) modulates immune environment via regulating macrophages and subsequently enhances osteogenesis, JBIC, J. Biol. Inorg. Chem. 24 (5) (2019) 733–745.
[31] Z. Chen, T. Klein, R.Z. Murray, R. Crawford, J. Chang, C. Wu, Y. Xiao, Osteoimmunomodulation for the development of advanced bone biomaterials, Mater. Today 19 (6) (2016) 304–321.
[32] V. Malheiro, Y. Elbs-Glatz, M. Obarzanek-Fojt, K. Maniura-Weber, A. Bruinink, Harvesting pre-polarized macrophages using thermo-responsive substrates, Sci. Rep. 7 (1) (2017) 42495.
[33] K. Igarashi, M. Hirafuji, H. Adachi, H. Shinoda, H. Mitani, Role of endogenous PGE2 in osteoblastic functions of a clonal osteoblast-like cell, MC3T3-E1, Prostaglandins Leukot. Essent. Fat. Acids 50 (4) (1994) 169–172.
[34] G. Girasole, R. Jilka, G. Passeri, S. Boswell, G. Boder, D. Williams, S. Manolagas, 17 beta-estradiol inhibits interleukin-6 production by bone marrow-derived stromal cells and osteoblasts in vitro: a potential mechanism for the antiosteoporotic effect of estrogens, J. Clin. Invest. 89 (3) (1992) 883–891.
[35] T. Kon, T.-J. Cho, T. Aizawa, M. Yamazaki, N. Nooh, D. Graves, L.C. Gerstenfeld, T. A. Einhorn, Expression of osteoprotegerin, receptor activator of NF-κB ligand (Osteoprotegerin Ligand) and related proinflammatory cytokines during fracture healing, J. Bone Miner. Res. 16 (6) (2001) 1004–1014.
[36] R. Johnson, B. Boyce, G. Mundy, G. Roodman, Tumors producing human tumor necrosis factor induce hypercalcemia and osteoclastic bone resorption in nude mice, Endocrinology 124 (3) (1989) 1424–1427.
[37] Q.-Z. Zhang, W.-R. Su, S.-H. Shi, P. Wilder-Smith, A.P. Xiang, A. Wong, A. L. Nguyen, C.W. Kwon, A.D. Le, Human gingiva-derived mesenchymal stem cells elicit polarization of M2 macrophages and enhance cutaneous wound healing, Stem Cells 28 (10) (2010) 1856–1868.
[38] D.J. Prockop, Concise review: two negative feedback loops place mesenchymal stem/stromal cells at the center of early regulators of inflammation, Stem Cells 31 (10) (2013) 2042–2046.
[39] F. Zhang, L.-F. Ren, H.-S. Lin, M.-N. Yin, Y.-Q. Tong, G.-S. Shi, The optimal dose of recombinant human osteogenic protein-1 enhances differentiation of mouse osteoblast-like cells: an in vitro study, Arch. Oral Biol. 57 (5) (2012) 460–468.
[40] E.-C. Kim, T.-H. Kim, J.-H. Jung, S.O. Hong, D.-W. Lee, Enhanced osteogenic differentiation of MC3T3-E1 on rhBMP-2-immobilized titanium via click reaction, Carbohydr. Polym. 103 (2014) 170–178.
[41] S. Ni, D. Zhai, Z. Huan, T. Zhang, J. Chang, C. Wu, Nanosized concave pit/convex dot microarray for immunomodulatory osteogenesis and angiogenesis, Nanoscale 12 (31) (2020) 16474–16488.
[42] H. Xing, R. Li, Y.A. Qing, B. Ying, Y. Qin, Biomaterial-based osteoimmunomodulatory strategies via the TLR4-NF-κB signaling pathway: a review, Appl. Mater. Today 22 (2021), 100969.
[43] P. Neacsu, A. Mazare, P. Schmuki, A. Cimpean, Attenuation of the macrophage inflammatory activity by TiO_2 nanotubes via inhibition of MAPK and NF-κB pathways, Int. J. Nanomedicine 10 (2015) 6455–6467.
[44] X. Shen, Y. Yu, P. Ma, Z. Luo, Y. Hu, M. Li, Y. He, Y. Zhang, Z. Peng, G. Song, K. Cai, Titania nanotubes promote osteogenesis via mediating crosstalk between macrophages and MSCs under oxidative stress, Colloids Surf. B: Biointerfaces 180 (2019) 39–48.